J. Anat. (2006) **208**, pp659–670

Habitual use of the primate forelimb is reflected in the material properties of subchondral bone in the distal radius

Kristian J. Carlson[1] and Biren A. Patel[2]

[1]*Department of Anatomical Sciences, School of Medicine, and* [2]*Interdepartmental Doctoral Program in Anthropological Sciences, Stony Brook University, USA*

Abstract

Bone mineral density is directly proportional to compressive strength, which affords an opportunity to estimate *in vivo* joint load history from the subchondral cortical plate of articular surfaces in isolated skeletal elements. Subchondral bone experiencing greater compressive loads should be of relatively greater density than subchondral bone experiencing less compressive loading. Distribution of the densest areas, either concentrated or diffuse, also may be influenced by the extent of habitual compressive loading. We evaluated subchondral bone in the distal radius of several primates whose locomotion could be characterized in one of three general ways (quadrupedal, suspensory or bipedal), each exemplifying a different manner of habitual forelimb loading (i.e. compression, tension or non-weight-bearing, respectively). We employed computed tomography osteoabsorptiometry (CT-OAM) to acquire optical densities from which false-colour maps were constructed. The false-colour maps were used to evaluate patterns in subchondral density (i.e. apparent density). Suspensory apes and bipedal humans had both smaller percentage areas and less well-defined concentrations of regions of high apparent density relative to quadrupedal primates. Quadrupedal primates exhibited a positive allometric effect of articular surface size on high-density area, whereas suspensory primates exhibited an isometric effect and bipedal humans exhibited no significant relationship between the two. A significant difference between groups characterized by predominantly compressive forelimb loading regimes vs. tensile or non-weight-bearing regimes indicates that subchondral apparent density in the distal radial articular surface distinguishes modes of habitually supporting of body mass.

Key words anthropoid; computed tomography osteoabsorptiometry (CT-OAM); locomotor behaviour; weight-bearing; wrist joint.

Introduction

Joints are a crucial adaptation in the vertebrate *bauplan* as they create greater capacities for performing movements. A segmented skeleton creates additional functional challenges, however, such as the need to transfer mechanical loads across joints. Although direct measurement of *in vivo* mechanical load is possible for certain parts of skeletal elements, such as long bone diaphyses (Lanyon et al. 1975; Burr et al. 1996; Demes et al. 1998, 2001), the use of strain gauges or load cells to measure *in vivo* forces in joint surfaces would compromise their structural integrity by disrupting articular cartilage. Thus, alternative methods are required for estimating force transmitted through articular surfaces.

The magnitude of force that crosses a joint often is assessed by quantifying trabecular architecture underlying the subchondral bone of an articular surface (e.g. Fyhrie & Carter, 1986; Carter et al. 1987, 1989; Pidaparti & Turner, 1997; Fajardo & Müller, 2001; Ryan & van Rietbergen, 2005). Relatively less attention has been directed toward subchondral cortical bone of a joint (but see Müller-Gerbl et al. 1989, 1990, 1992; Eckstein et al. 1995, 1999). Because compressive strength of bone is directly proportional to its mineral content (Vose

Correspondence
Dr K. J. Carlson, Anthropologisches Institut und Museum, Universität Zürich, Winterthurerstrasse 190, 8057 Zürich, Switzerland. T: +41 44 6355415; F: +41 44 6356804; E: carlson@aim.unizh.ch (KJC), bapatel@ic.sunysb.edu (BAP).

Accepted for publication *5 January 2006*

& Kubala, 1959; Ascenzi & Bonucci, 1967, 1968, 1972; Currey, 1969a,b), mineralization of the subchondral cortical plate in an articular surface may reflect the 'loading history' experienced by a joint, where mineral distribution reflects a materialized field of stress caused by the distribution of loads over the entire joint surface (Pauwels, 1965). Müller-Gerbl et al. (1989, 1992) pioneered the use of computed tomography osteoabsorptiometry (CT-OAM) to assess such patterns in subchondral cortical plates of synovial joints. Radiographic methods such as CT-OAM factor tissue (e.g. mineralized matrix) and internal spaces (e.g. Haversian canals and lacunae) into output (e.g. Hounsfield units). Thus, optical densities, which are visualized as white, black and 254 intermediate shades of grey, are most analogous to measures of apparent density because internal spaces are included, i.e. bulk mass per unit volume. CT-OAM has proven to be quite successful in assessing 'long-term stress distribution in the subchondral bone' (Eckstein et al. 1999: 96), as indicated by its adoption in subsequent clinical studies of human shoulder (Müller-Gerbl et al. 1990; Oizumi et al. 2003), elbow (Eckstein et al. 1995), wrist (Iwasaki et al. 2000; Hoogbergen et al. 2002; Giunta et al. 2004), metacarpophalangeal (Meirer et al. 2004), hip (von Eisenhart-Rothe et al. 1997), knee (Müller-Gerbl et al. 1992), ankle (Müller-Gerbl et al. 1989) and tarsometatarsal joints (Linsenmaier et al. 2003).

Several studies have noted an association between bone mineralization and human performance activities (e.g. Kannus et al. 1994; Haapasalo et al. 1998; Heinonen et al. 1998; Kontulainen et al. 1999; Taaffe & Marcus, 1999; Proctor et al. 2002; see recent review in Pearson & Lieberman, 2004). Fewer studies, by comparison, have investigated analogous relationships among non-human primates (e.g. Burr, 1979a,b; Schaffler & Burr, 1984; DeRousseau, 1988; Ahluwalia, 2000; Carlson, 2002, 2003; Kikuchi et al. 2003; Patel & Carlson, 2005). Non-human primates exhibit a wide spectrum of locomotor behaviours that potentially involve vastly different loading regimes. For example, forelimbs can be used to support body mass above substrates, or to suspend body mass beneath superstrates (Hunt et al. 1996; Fleagle, 1999). Primate locomotor diversity therefore provides a 'natural experiment' for assessing subchondral apparent density in relation to habitual loading in forelimb joints.

By extending CT-OAM beyond human clinical research, issues regarding primate locomotion and bone material properties can be addressed. Supporting body mass above substrates, on the one hand, creates predominantly compressive loads during quadrupedalism owing to joint reaction forces arising both from contraction of muscles that bridge the joint and from gravitational forces operating on the supported body mass. Suspending body mass from superstrates, on the other hand, restricts joint reaction forces generated from forelimb compressive loads primarily to those originating from muscle contractions. Humans are unique among primates as the adoption of a habitual bipedal gait frees the forelimb from any body mass support function, leaving only joint reaction forces that arise from muscle contractions.

The distal radius is a critical location in which to investigate the transmission of force through the forelimb because among many vertebrates, particularly primates, it contributes a majority of the forearm articular surface in the wrist joint. The wrist (i.e. radiocarpal joint) has more congruous articular surfaces in comparison with other forelimb joints (e.g. the elbow), thus minimizing the presence of bending loads experienced by subchondral bone and warranting application of the CT-OAM approach (Eckstein et al. 1999). Given the diverse array of behavioural repertoires exhibited by free-ranging non-human primates (e.g. quadrupedalism vs. suspensory locomotion), subchondral apparent density of the distal radius may be quite variable among taxa. The goal of the present study is to evaluate the primate distal radius for patterns in such potential variation. This will improve current understanding of habitual loading and force transmission through the primate wrist by providing additional data on morphological manifestations of habitual forelimb loading regimes.

Two specific questions are addressed here. Acknowledging that some intragroup variation in apparent density may be expected as a result of demographic factors such as age and sex, do groups characterized by relatively more habitual compressive forelimb loading (e.g. quadrupedal primates) exhibit more area of high apparent density, whereas groups exhibiting relatively less habitual compressive forelimb loading (e.g. suspensory and bipedal primates) exhibit less area of high apparent density? In addition to comparing the extent of areas of high apparent density, distribution of such areas may differ between groups. Thus, the second question is whether groups such as quadrupedal primates that experience more habitual forelimb compressive loads display more concentrated areas of high apparent density in the distal radial articular surface, whereas groups such as suspensory and bipedal primates that experience

less habitual compressive forelimb loads display more diffuse areas of high apparent density?

Materials and methods

Sample selection

The comparative sample consisted of 55 right radii from adult specimens (Table 1). Only specimens that exhibited epiphyseal closure on all observable long bones were used. Growing individuals normally exhibit lower apparent density of bone than adult individuals based on age differences alone (Martin et al. 1998; Currey, 2002). Of the available adult specimens, specimens exhibiting signs of degenerative joint disease (e.g. osteophytes around articular margins, eburnation on articular surfaces or marginal lipping of joints) were avoided (Ortner & Putschar, 1981). Osteophytes are particularly diagnostic of osteoarthroses (OA) (Amir et al. 1992). Specimens also were excluded when exhibiting traumatic injury in the postcranial skeleton; when distal radial articular surfaces were abraded postmortem; and when specimens were excessively greasy. The presence of significant grease can alter optical density values acquired through radiography (Ruff & Leo, 1986). Females and males were pooled within taxa for two reasons. First, sexual dimorphism in behavioural repertoires within quadrupedal, suspensory or bipedal taxa is not as distinct as behavioural differences between females or males of any two of these taxa (Fleagle, 1999). Furthermore, specimen sex was not always reported in museum records, nor was it estimated readily from skeletal indicators in monomorphic primate taxa (e.g. *Hylobates*).

Digital data acquisition

Medical CT was used to generate digital images of distal radii. A GE Lightspeed 16 medical CT scanner was used to acquire data from a majority of the samples, while a second scanner was used for acquiring data from four *Pongo pygmaeus* specimens (Siemens Somatom AR™). Relevant scanning parameters on GE/Siemens scanners included tube voltage, 120 kV/110 kV; tube current, 70 mA/63 mA; and scan time, 1.0 s/1.3 s. All radii were scanned and reconstructed such that only one radius appeared within the field of view (FOV). This was necessary as optical density values were desired and inclusion of more than one specimen within the FOV potentially lessens the range of grey values representing a specimen. In other words, when two specimens are included within the FOV, only one specimen will establish the maximum grey value. All image reconstructions were made using a standard reconstruction algorithm (e.g. abdomen) rather than a bone algorithm. We chose a standard algorithm because bone algorithms artificially inflate Hounsfield units of pixels at steep gradients (i.e. bone edges), which in turn would alter optical densities.

We used the following slice thicknesses during image data acquisition: GE (0.625 mm) and Siemens (1.0 mm). Ideally, slice thickness could be held constant to promote similar precision in modelling articular surfaces, but different manufacturer specifications often require

Table 1 Comparative sample details

Taxon	*n*	Source	Gait category	Avg. body mass (kg)*
Homo sapiens	10	SBU	Bipedal	
Pongo pygmaeus	5	AMNH, NMNH	Suspensory	♀ = 35.8; ♂ = 78.5
Hylobates hoolock	7	AMNH	Suspensory	♀ = 6.9; ♂ = 6.9
Gorilla gorilla	6	AMNH	Quadrupedal	♀ = 71.5; ♂ = 170.4
Pan troglodytes	5	AMNH, RS	Quadrupedal	♀ = 33.7; ♂ = 42.7
Cercopithecus neglectus	3	RS	Quadrupedal	♀ = 4.1; ♂ = 7.4
Colobus guereza	4	AMNH	Quadrupedal	♀ = 9.2; ♂ = 13.5
Erythrocebus patas	2	AMNH	Quadrupedal	♀ = 6.5; ♂ = 12.4
Mandrillus sphinx	3	AMNH	Quadrupedal	♀ = 12.9; ♂ = 31.6
Nasalis larvatus	3	AMNH	Quadrupedal	♀ = 9.8; ♂ = 20.4
Papio ursinus	7	AMNH, RS	Quadrupedal	♀ = 14.8; ♂ = 29.8

AMNH = Department of Mammology, American Museum of Natural History, New York, NY, USA; NMNH = Department of Mammology, National Museum of Natural History (Smithsonian), Washington, DC, USA; RS = Randall Susman private collection; SBU = Gabor Inke Anatomical Sciences Laboratory, School of Medicine, Stony Brook University, Stony Brook, NY, USA.
*Reported in Smith & Jungers (1997).

different slice thicknesses, as was the case here. The FOV was minimized to the maximum extent possible while safely ensuring that complete articular surfaces were captured: values ranged from 95 to 100 mm for all but three specimens *Pongo*. We recommend using the minimum allowable slice thickness and FOV values in order to partition articular surfaces into as many pixels as possible. This is useful for identifying precise differences in apparent density patterns, as well as for identifying bone–air boundaries when using a standard filter.

A sheet of foamed polystyrene (e.g. Styrofoam®) 3.0 cm in thickness was placed directly on the scanner bed, levelled with standard built-in devices available in CT scanners (i.e. lasers or lights), and temporarily attached to the bed so that further positioning could be accomplished from the scanner console. Bones were positioned on the levelled sheet such that their distal articular surface was perpendicular to the scan plane. Thus, scan planes effectively became sagittal planes of diaphyses rather than coronal planes (for further details see Ahluwalia, 2000). Because minimum slice thickness settings are dependent upon CT manufacturer, and can exceed the thickness of the subchondral cortical plate in taxa of smaller body sizes, sagittal scan planes help reduce partial volume averaging artefacts when representing depth of the subchondral cortical plate. Because pixel dimensions (i.e. width and height) are dependent upon FOV rather than slice thickness, it is possible to use even more precision in modelling the depth of the subchondral plate by adopting this protocol (e.g. minimum depth of 0.188 mm in a sagittal plane vs. 0.625 mm in a coronal plane). All images were inspected after acquisition for scanning artefacts such as 'streaking' and beam hardening (Zollikofer & Ponce de León, 2005).

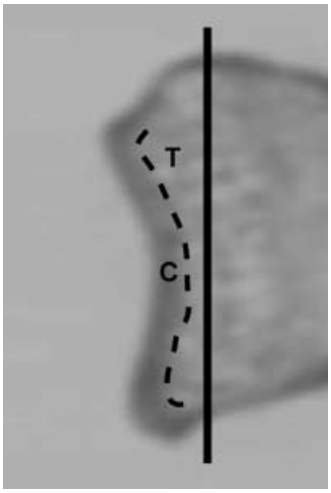

Fig. 1 Magnified sagittal view of a distal radius. 'C' indicates the subchondral cortical plate. 'T' indicates trabecular bone underlying the plate. A dashed line indicates the approximate border between these two regions of subchondral bone. The proximal location along which images were cropped is located approximately at the solid vertical line. Although trabecular bone could not be eliminated entirely, trabecular bone has a lower apparent density relative to (subchondral) cortical bone, making it unlikely that underlying trabecular bone would set values in maximum intensity projections (Martin et al. 1998).

Image analysis

Digital images were imported into ImageJ software, which is available as a free download at http://rsb.info.nih.gov/ij. The distal articular surface of the radius was cropped from each image in a series such that most underlying trabecular bone was excluded from analyses (Fig. 1). Cropped images were stacked, digitally re-sliced in a direction perpendicular to the original plane of section, then rotated 90° such that the articular surface could be viewed. A maximum intensity projection (MIP) map was constructed from each re-sliced and rotated stack. A MIP represents a three-dimensional (3D) data volume (voxels) compressed into a 2D image (pixels) in which each pixel represents the maximum brightness value (i.e. optical density) achieved along a line of sight leading through those voxels in the same line perpendicular to a pixel in the 2D image plane. Although some trabecular bone immediately underlying the subchondral cortical plate could not be excluded during subsequent steps, this would not factor into MIP brightness values as trabecular bone is known to exhibit lower apparent density than (subchondral) cortical bone (Martin et al. 1998).

After generating the MIP, optical density patterns were visualized using false-colour maps restricted to eight colours (Fig. 2). Each colour represented a range of 32 grey values (except white, which was 31) where the lowest bin (white) represented the lowest optical densities (e.g. grey values 224–254) and the highest bin (black) represented the highest optical densities (e.g. grey values 0–31). Background pixels in the image (e.g. grey values of 255) were subtracted before pixel counting. False-colour maps of MIPs were projected onto corresponding virtual reconstructions of distal radii that were generated using Slicer 3D software (www.slicer.org). This provided a reliable means of

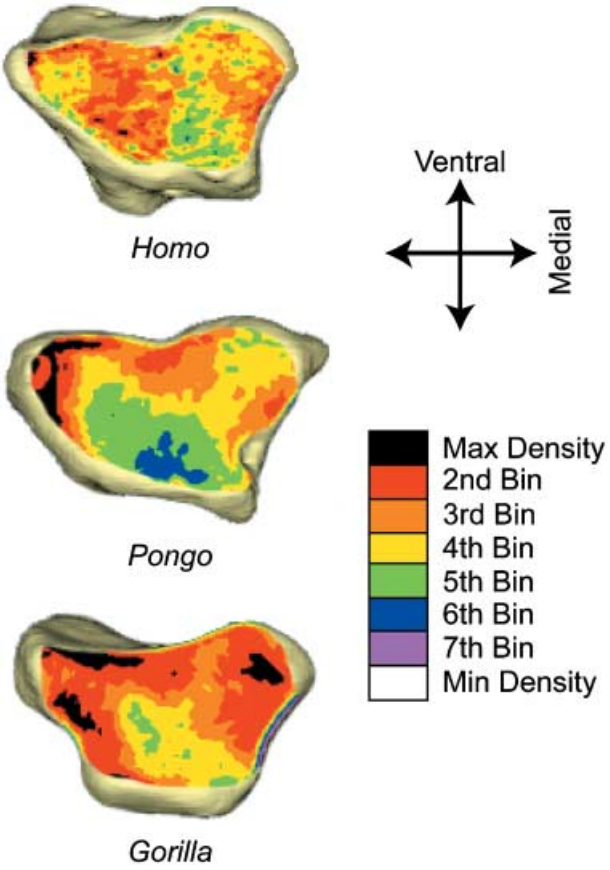

Fig. 2 Maximum intensity projection (MIP) maps for radii superimposed upon 3D virtual reconstructions of the same distal radii. The three images from top to bottom are: a human, representing a bipedal primate; an orang utan (*Pongo pygmaeus*), representing a suspensory primate, and a gorilla (*Gorilla gorilla*), representing a quadrupedal primate. Note the relative absence of high apparent density area in the human (black pixels), while the orang utan has an intermediate area in comparison with the human and the gorilla. Also note the tendency for the orang utan and gorilla to exhibit more defined clusters of high apparent density area (black pixels), while the high apparent density area is more dispersed in the human. Images are scaled to the same size for the sake of visual comparisons.

identifying articular surface boundaries in false-colour maps. Once an articular surface was identified in an MIP, extraneous areas of the MIP were removed by using manual eraser tools available in Adobe® Photoshop®. Subsequently, MIPs were subjected to pixel counting procedures.

Statistical analysis

In order to assess the size and concentration of areas of high apparent density, MIPs were compared between locomotor groups. The pixels in each of the eight bins (i.e. colours) were counted using custom-written macros for ImageJ and commercial spreadsheet software (e.g. MS Excel). The sum of all bins was recorded as the number of pixels in the articular surface. Areas were quantified as the percentage of pixels in a given bin relative to the number of pixels in a given articular surface. Comparing percentages is more appropriate than comparing raw pixel counts because pixel sizes occasionally varied between specimens for reasons previously stated (e.g. different CT parameters). In addition, an individual with more pixels in the articular surface (e.g. larger articular surface) could exhibit more pixels in the highest bin (i.e. black) simply because there are more overall pixels within the articular surface. Group differences in mean percentages were evaluated with Student's *t*-tests. Reduced major axis (RMA) regression was used to investigate potential group differences in the effect of articular surface size on the number of high-density pixels.

In order to assess whether high apparent density was concentrated or diffuse, we defined a cluster using three criteria: (1) pixels in the cluster had to be in the highest range of the false-colour map (i.e. black), (2) pixels in the cluster had to be adjacent, by sharing at least a side or a corner, and (3) the number of pixels in the cluster had to exceed 1% of the total number of pixels in the articular surface. Counting pixels in a cluster was performed in ImageJ by setting the scale to measure in pixels (i.e. not mm per pixel), using the wand tool to select adjoining black pixels, and then using the measure option. Although the choice of cutoff value (1%) was somewhat arbitrary, it corresponded with qualitative assessments as to what appeared to be a discrete cluster vs. a random scatter. Concentrations were ordinal data, and thus non-parametric Mann–Whitney *U*-tests were used to evaluate group differences in the number of concentrations.

Statistical significance was assigned when $P < 0.05$. Student's *t*-tests and Mann–Whitney *U*-tests were performed in SPSS 11.0 (SPSS, Chicago, IL, USA). RMA regression routines and tests were calculated using the program (S)MATR (Falster et al. 2003).

Results

Relative extent of apparent density

Patterns of subchondral apparent density in the articular surface of the distal radius differed between groups

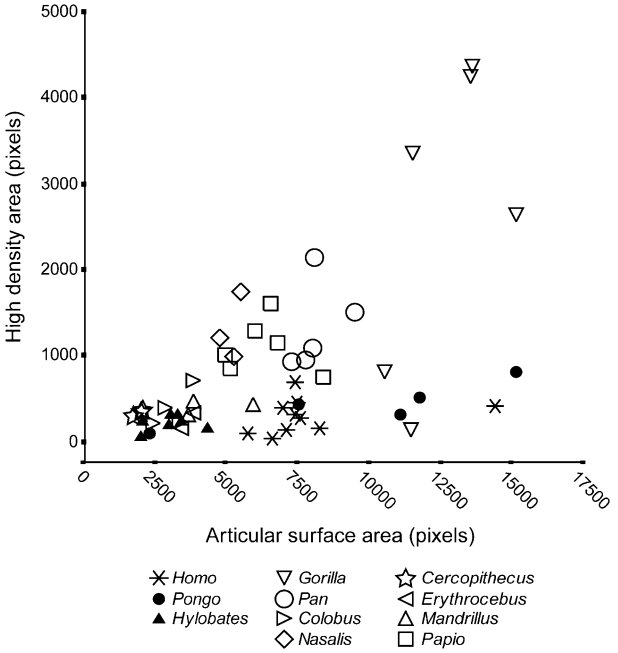

Fig. 3 Scatter plot of high apparent density area (pixels in the black bin) vs. the overall 2D articular surface area (pixels in the articular surface). Bipedal primates are depicted by asterisks, suspensory primates by solid symbols and quadrupedal primates by open symbols.

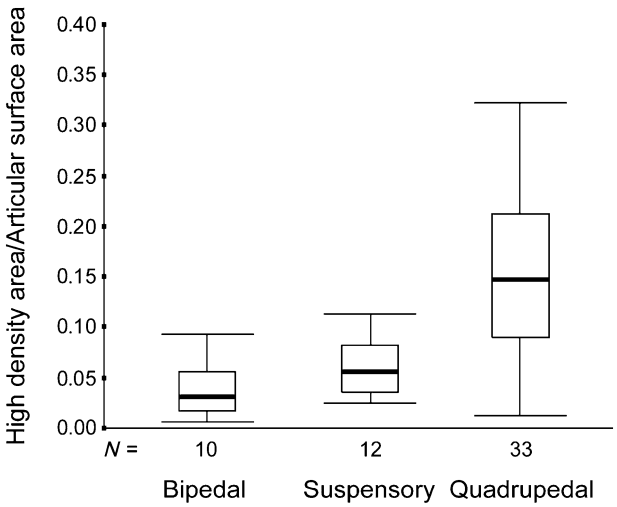

Fig. 4 Box and whiskers plot of the high apparent density area (pixels in the black bin) as a percentage of the overall 2D articular surface area (pixels in the articular surface). Boxes contain 50% of the observed values for each group. Thick horizontal lines (within boxes) indicate group median values. Vertical lines extending outwards from boxes indicate extreme high and low values observed for each group. Note that group differences in high apparent density area remain apparent even after adjusting for the size of articular surfaces.

(Table 2, Figs 2 and 3). Groups with larger articular surfaces exhibited tendencies towards greater area of high apparent density (i.e. black pixels), although this trend was less obvious in suspensory (closed symbols) and bipedal (asterisks) primates than in quadrupedal primates (Fig. 3). However, even after controlling for potential articular surface size effects (i.e. by comparing percentage maximum pixels), group differences in the extent of high apparent density remained readily apparent (Fig. 4).

Quadrupedal primates generally had the most proportionately extensive area of high apparent density, whereas suspensory and bipedal groups exhibited proportionately more articular surface area with lower apparent density, e.g. areas represented by bins 2–5 (Table 2). When comparing percentages of areas of high apparent density within articular surfaces, suspensory and bipedal primates exhibited significantly smaller areas than quadrupedal primates (Table 3). Percentage area of high apparent density in bipedal primates was smaller relative to that in suspensory primates, but the difference between the group percentages was not statistically significant (Table 3).

Table 2 Apparent density areas represented by pixels in maximum intensity projections

	Total pixels	% max	% 2nd	% 3rd	% 4th	% 5th	% 6th	% 7th	% min	No. of concentrations
Bipedal $n = 10$	7916.5 (2379.5)	3.7 (2.6)	16.0 (7.9)	28.3 (6.5)	28.3 (6.4)	14.9 (8.9)	3.6 (2.4)	1.8 (0.3)	3.4 (0.5)	0.4 (0.5)
Suspensory $n = 12$	5777.0 (4509.7)	6.0 (2.9)	17.9 (7.2)	30.2 (8.0)	25.7 (7.7)	9.9 (8.6)	3.1 (1.8)	2.3 (0.5)	4.8 (1.3)	1.3 (0.8)
Quadrupedal $n = 33$	6528.6 (3589.3)	16.2 (8.2)	23.3 (10.7)	27.3 (7.4)	19.8 (11.7)	5.3 (4.1)	2.1 (1.0)	1.9 (0.7)	4.1 (1.4)	2.0 (1.0)

Values are mean (1 SD). Percentages were calculated as the number of pixels in a bin divided by the total number of pixels in the articular surface.

Table 3 Pairwise comparisons for percentages of high apparent density area within articular surfaces

	t	d.f.	*P*
Bipedal vs. Suspensory	–1.887	20	0.074
Bipedal vs. Quadrupedal†	–7.544	40.730	< 0.001*
Quadrupedal vs. Suspensory†	6.156	42.998	< 0.001*

*Significant at $P < 0.001$ (two-tailed).
†Assuming unequal variances as the comparison failed a Levene test for equality of variances.

The bivariate relationship between logged high-density area (i.e. black pixel counts) and logged articular surface size (i.e. total pixel counts) did not explain a significant amount of variation within the observed values of the bipedal group, unlike for either quadrupedal or suspensory groups (Table 4). The difference in significance could be influenced by a greater range of articular surface sizes in the quadrupedal and suspensory groups resulting from combining taxa (Table 2, Fig. 3). The suspensory group exhibited a slope that was not significantly different from isometry, whereas the quadrupedal group exhibited a slope significantly greater than 1 (Table 4). Thus, there was a positive allometric effect between articular surface size and area of high apparent density among quadrupeds only. Given these differences, it is not surprising that group RMA slopes were heterogeneous (i.e. no common slope existed for bipedal, suspensory and quadrupedal primates) (Test statistic = 8.449, $P = 0.010$).

Relative concentration of apparent density

Discrete areas of high apparent density in articular surfaces were more numerous in the quadrupedal group (i.e. African apes and monkeys) than in bipedal primates (i.e. humans), whereas suspensory primates (i.e. *Pongo* and *Hylobates*) exhibited an intermediate number (Table 2). Paired comparisons of group mean counts revealed that each group showed significant differences in mean concentration numbers from other groups (Table 5).

Discussion

Apparent density of subchondral bone in the distal articular surface of the radius discriminated habitual loads in the primate wrist joint, specifically the radiocarpal joint. Three groups of primates – bipedal, suspensory and quadrupedal – were differentiated. A 'natural experiment' comparing the relative amount of area of high apparent density in these three groups, as well as the distribution of these areas, demonstrated significant group differences, presumably due to different forelimb loading regimes. The presence of a functional signal in subchondral apparent density of the primate distal radius is consistent with previous studies that have identified a functional signal in bone material properties from other skeletal locations (e.g. Burr, 1979a,b; Schaffler & Burr, 1984; DeRousseau, 1988; Ahluwalia, 2000).

Table 4 Reduced major axis regression results for logged maximum pixels regressed on logged total pixels in articular surface

Group	Slope	95% CI	Intercept	R^2	*P*	*F**	*P**
Bipedal	3.54	1.78–7.03	–11.390	0.171	0.235	–	–
Suspensory	1.06	0.69–1.64	–1.488	0.593	0.003	0.082	0.780
Quadrupedal	1.64	1.27–2.11	–3.257	0.515	< 0.001	16.901	< 0.001

95% CI = 95% Confidence Interval for slope.
*Test results comparing individual group RMA slopes with the theoretical value for isometry (1). Note that the bipedal group was not compared with the theoretical value for isometry as the relationship between logged maximum pixels and logged total pixels was non-significant.

Table 5 Pairwise comparisons for concentrations of high apparent density area within articular surfaces

	Mean ranks	Mann–Whitney *U*-statistic	*P*
Bipedal vs. Suspensory	B = 7.8; S = 14.6	23.0	0.007**
Bipedal vs. Quadrupedal	B = 8.2; Q = 26.2	27.0	< 0.001**
Quadrupedal vs. Suspensory	Q = 25.7; S = 15.6	109.5	0.017*

*Significant at $P < 0.05$ (two-tailed); **significant at $P < 0.001$ (two-tailed).

African apes and monkeys (i.e. quadrupedal primates), which predominantly support their body mass on substrates such that this mass generates a habitual compressive force in the forelimb, collectively exhibited both greater area of high apparent density and more discrete concentrations of these areas as compared with the suspensory and bipedal groups. The significance of this pattern was robust despite substantial differences in the amount of observed intragroup variation. It is noteworthy that individuals within any given taxon, including quadrupeds, were frequently similar in their area of high apparent density (Table 2, Fig. 2). This suggests that interspecific trends are visible despite the likelihood of intraspecific variation due to factors such as age and sex. Understanding the basis of potential intraspecific variation in subchondral density patterns would be worthwhile as modelling and remodelling rates are known to vary with age, while hormonal differences between adult males and females also probably affect material properties of subchondral bone by modulating remodelling rates (Martin et al. 1998). Although it is conceivable that variation among quadrupeds could be attributable to having a larger sample, there are potential functional explanations worth considering. For example, quadrupedal primates exhibit variable forms of habitual hand postures during terrestrial locomotion (e.g. digitigrady, palmigrady, knuckle-walking), each of which could impact subchondral apparent density in the distal radial articular surface differently. This could contribute to higher variability in subchondral apparent density patterns within quadrupedal primates relative to suspensory and bipedal primate groups. We are actively investigating this possibility.

Suspensory primates habitually use their forelimbs to suspend their body mass from superstrates such that their forelimbs experience a predominantly tensile force (Swartz et al. 1989). This effectively limits compressive loads experienced by subchondral bone of their distal radius to those caused by muscle contractile forces (e.g. digital flexors). Compared with quadrupedal primates, suspensory primates exhibited relatively less area of high apparent density, as well as a relatively more diffuse area of high apparent density. Bipedal primates, which do not typically involve their forelimb during support of body mass, were convergent on suspensory primates in their relative amount of high apparent density. Taken in the context of the difference either of these groups exhibited relative to the quadrupedal group, the similarity between suspensory and bipedal primates could suggest that habitual tensile loading and non-weight-bearing loading of the forelimb, respectively, do not differentiate relative amounts of high apparent density areas of subchondral bone in the distal radial articular surface. This lack of differentiation, however, did not extend to discrete clusters of high apparent density area as suspensory primates exhibited significantly more clusters than bipedal primates.

What would seem to be less substantial or absent compressive joint reaction forces, respectively arising from supporting body mass in suspensory and bipedal primates relative to quadrupedal primates suggests that the effect of the joint reaction force due to muscle contraction is isolated more readily in the former two groups. *Pongo* and *Hylobates* have massively muscled forelimbs relative to humans (Tuttle, 1972). Similar proportionate areas of high apparent density in suspensory and bipedal primates, however, indicate that muscle contractile forces may not have a significant impact on subchondral apparent density in the distal radial articular surface, or at least that this signal is less dominant than the signal attributed to compressive joint reaction forces arising from support of body mass on substrates (i.e. weight-bearing). Interestingly, this is counter to the idea that muscle forces have greater contributions than body weight when considering whole-bone strength (Frost, 2001).

Although discussion of a functional signal thus far has emphasized a positive association between the magnitude/frequency of compressive loading of the distal radial articular surface and its apparent density, proximate tissue-level mechanisms (e.g. fluid flow gradients) ultimately must be considered. Consider, for example, Frost's Mechanostat hypothesis in which minimum effective strain (MES) for the remodelling threshold operates via a negative feedback mechanism (Frost, 1990a,b, 2001; Skedros et al. 2001). When strain magnitude falls below a remodelling threshold, bone turnover is initiated. Increased bone turnover is associated both with higher porosity because Haversian canals become more numerous during remodelling and with new matrix that has a lower mineral content relative to the replaced mature matrix (Martin et al. 1998; Currey, 2002). Both porosity and mineral content factor into measurements of apparent density. Suppression and initiation of remodelling may even be a local phenomenon within an articular surface. Histomorphometric studies of subchondral bone in the distal radius of

these groups, however, are necessary in order to clarify which material properties (e.g. porosity or mineralization) could be most responsible for the observed patterns in apparent density.

Collagen fibre orientation reflects habitual loading regimes in cortical bone (de Margerie, 2002; Skedros et al. 2003). Collagen fibres are predominantly longitudinal when tensile loads are high and transverse when compressive loads are high. Typically, collagen fibre orientation is determined by observing different opacities in bone thin sections. Collagen fibre orientation, however, was beyond the scope of the present study because CT-OAM, as a radiographic method, does not provide an accurate means of quantifying it. It is at least plausible, however, that collagen fibre orientation could have a role in mediating observed subchondral apparent density differences between the three groups.

In early studies of osteoarthrosis (OA), increased apparent density of subchondral bone was proposed to increase stress in the overlying articular cartilage (Radin et al. 1970, 1972). Radin and colleagues suggested that a lack of accommodation to impact stresses over time resulting from the increased stiffness of subchondral bone overwhelmed self-repair mechanisms of the articular cartilage, thus leading to the onset of OA. Subsequent studies of OA pathogenesis have suggested that mineral density of the subchondral cortical plate decreases as bone turnover increases, but that thickness of the subchondral bone plate increases (Grynpas et al. 1991; Burr & Radin, 2003; Bailey et al. 2004). In fact, debate continues over whether alterations in subchondral bone precede the initial degeneration of articular cartilage, or whether they occur subsequent to the onset of this degeneration (Carlson et al. 1996; Dequeker & Luyten, 2000; Day et al. 2004; Wang et al. 2005). Although our study was not designed to address OA pathogenesis explicitly (cf. DeRousseau, 1988), examining subchondral variability within non-human primates of variable locomotor types helps to address 'the lack of information about joint tissue adaptation and disease [that] has hampered objective studies of osteochondral tissues' (Kawcak et al. 2001).

Given that the sample was derived from multiple sources, it was not possible to standardize the manner in which radii were harvested from specimens, nor were radii stored under ideal conditions for studying bone material properties (e.g. frozen and/or placed in solution upon harvesting). Nearly all specimens came from a single museum collection, however, which minimized variation in specimen treatment protocol to some extent (Table 1). In addition, it is important to note that relatively little intraspecific variation was observed among either the five *Pongo* or the seven *Papio* specimens, both of which were represented by specimens from multiple sources and incorporated the full range of FOV values (see Fig. 3). The small amount of intragroup variation in these taxa suggests that the functional signal in subchondral apparent density is relatively robust to specimen treatment and slight variations in CT parameters, and that CT-OAM can be applied to specimens from museum collections.

Extending patterns in apparent density of subchondral bone to additional taxa may offer further insights into the nature of joint loading regimes. For instance, investigation of other primate and non-primate taxa would be a worthwhile pursuit, as would be the investigation of additional articular surfaces in these taxa (e.g. DeRousseau, 1988). The distal radial articular surface in two primate vertical clinger/leaper (VCL) individuals (*Indri indri* = 10.1% max., *Propithecus diadema* = 7.7% max.), when compared with corresponding values in Table 2, provides preliminary evidence that VCLs resemble suspensory primates (mean % max. = 6.0) more than quadrupedal primates (mean % max. = 16.2), as would be expected based on their minimal forelimb involvement during take-off and landing from vertical substrates (Demes et al. 1996, 1999).

Applying this technique to fossil taxa may be useful if it can be shown that subchondral material properties can be studied in joint surfaces of fossil specimens. Although it is unclear whether inorganic mineral exchange during the fossilization process could leave intact mineralization gradients in subchondral bone, examining other material properties, or perhaps subchondral thickness, ultimately could prove to be useful. Because it is conceivable that variable subchondral thicknesses could attenuate X-rays differently, CT-OAM may provide a means of assessing localized thicknesses within articular surfaces. We currently are investigating this possibility in order to determine whether, and if so to what extent, patterns in subchondral bone thickness mirror observed patterns in subchondral apparent density for the distal radial articular surface.

Acknowledgements

Funding for this research was provided by Sigma Xi Grants-In-Aid of Research to B.A.P. We wish to express

our appreciation to the following people at the American Museum of Natural History, New York, and the National Museum of Natural History (Smithsonian), Washington, for making specimens available to us and for facilitating our data collection: Bruno Frohlich, Evan Garofalo, Linda Gordon, Ross MacPhee, Richard Monk, Nancy Simmons, Jean Spence and Eileen Westwig. We also wish to thank and acknowledge the co-operation of Randy Susman for granting access to specimens in his personal collection. We acknowledge the generous co-operation of Stony Brook University Hospital in granting access to CT facilities. We express our gratitude to Charlie Mazzarese, Wayne Mattera and Lou Caronia for their assistance in acquiring CT image data. We are indebted to the following people for various forms of assistance and sharing comments throughout the course of this research: Kamla Ahluwalia, Luci Betti-Nash, Brigitte Demes, Andy Farke, Justin Georgi, Stefan Judex, Bill Jungers, Susan Larson, Justin Sipla, Jesse Young and Christoph Zollikofer. Finally, we thank three anonymous reviewers and a receiving editor of the *Journal of Anatomy* for their comments and suggestions. We acknowledge one reviewer, in particular, for stimulating comments regarding the physiological mechanism behind the observed patterns in subchondral apparent density.

References

Ahluwalia K (2000) *Knee joint load as determined by tibial subchondral bone density: its relationship to gross morphology and locomotor behavior in catarrhines*. PhD Dissertation, Stony Brook University.

Amir G, Pirie CJ, Rashad S, Revell PA (1992) Remodeling of subchondral bone in osteoarthritis: a histomorphometric study. *J Clin Pathol* **45**, 990–992.

Ascenzi A, Bonucci E (1967) The tensile properties of single osteons. *Anat Rec* **158**, 375–386.

Ascenzi A, Bonucci E (1968) The compressive properties of single osteons. *Anat Rec* **161**, 377–391.

Ascenzi A, Bonucci E (1972) The shearing properties of single osteons. *Anat Rec* **172**, 499–510.

Bailey AJ, Mansell JP, Sims TJ, Banse X (2004) Biochemical and mechanical properties of subchondral bone in osteoarthritis. *Biorheology* **41**, 349–358.

Burr DB (1979a) Density variation in the humeral cortex of *Macaca*. *Am J Anat* **155**, 311–318.

Burr DB (1979b) Patterns of variability in mineralization of the primate femoral diaphysis. *Am J Phys Anthropol* **51**, 219–232.

Burr DB, Milgrom C, Fyhrie D, et al. (1996) *In vivo* measurement of human tibial strains during vigorous activity. *Bone* **18**, 405–410.

Burr DB, Radin EL (2003) Microfractures and microcracks in subchondral bone: are they relevant to osteoarthrosis? *Rheum Dis Clin N Am* **29**, 675–685.

Carlson CS, Loeser RF, Purser CB, Gardin JF, Jerome CP (1996) Osteoarthritis in cynomolgus macaques III: effects of age, gender, and subchondral bone thickness on the severity of disease. *J Bone Miner Res* **11**, 1209–1217.

Carlson KJ (2002) *Shape and material properties of African pongid femora and humeri: their relationship to observed positional behaviors*. PhD Dissertation, Indiana University, Bloomington.

Carlson KJ (2003) Mineral density patterns in femora and humeri of African pongids. *Am J Phys Anthropol Suppl* **35**, 74.

Carter DR, Fyhrie DP, Whalen RT (1987) Trabecular bone density and loading history: regulation of connective tissue biology by mechanical energy. *J Biomech* **20**, 785–794.

Carter DR, Orr TE, Fyhrie DP (1989) Relationships between loading history and femoral cancellous bone architecture. *J Biomech* **22**, 231–244.

Currey JD (1969a) The mechanical consequences of variation in the mineral content of bone. *J Biomech* **2**, 1–11.

Currey JD (1969b) The relationship between the stiffness and the mineral content of bone. *J Biomech* **2**, 477–480.

Currey JD (2002) *Bones: Structure and Mechanics*. Princeton, NJ: Princeton University Press.

Day JS, van der Linden JC, Bank RA, et al. (2004) Adaptation of subchondral bone in osteoarthritis. *Biorheology* **41**, 359–368.

Demes B, Jungers WL, Fleagle JG, Wunderlich RE, Richmond BG, Lemelin P (1996) Body size and leaping kinematics in Malagasy vertical clingers and leapers. *J Hum Evol* **31**, 367–388.

Demes B, Stern JT Jr, Hausman MR, Larson SG, McLeod KJ, Rubin CT (1998) Patterns of strain in the Macaque ulna during functional activity. *Am J Phys Anthropol* **106**, 87–100.

Demes B, Fleagle JG, Jungers WL (1999) Takeoff and landing forces of leaping strepsirhine primates. *J Hum Evol* **37**, 279–292.

Demes B, Qin Y, Stern JT Jr, Larson SG, Rubin CT (2001) Patterns of strain in the Macaque tibia during functional activity. *Am J Phys Anthropol* **116**, 257–265.

Dequeker J, Luyten FP (2000) Bone mass and osteoarthritis. *Clin Exp Rheumatol* **18** (Suppl. 21), S21–S26.

DeRousseau CJ (1988) Osteoarthritis in rhesus monkeys and gibbons: a locomotor model of joint degeneration. *Contrib. Primatol* **25**, 1–145.

Eckstein F, Müller-Gerbl M, Steinlechner M, Kierse R, Putz R (1995) Subchondral bone density of the human elbow assessed by CT osteoabsorptiometry: a reflection of the loading history of the joint surfaces. *J Orthop Res* **13**, 268–278.

Eckstein F, Merz B, Schön M, Jacobs CR, Putz R (1999) Tension and bending, but not compression alone determine the functional adaptation of subchondral bone in incongruous joints. *Anat Embryol* **199**, 85–97.

von Eisenhart-Rothe R, Eckstein F, Müller-Gerbl M, Landgraf J, Rock C, Putz R (1997) Direct comparison of contact areas, contact stress and subchondral mineralization in human hip joint specimens. *Anat Embryol* **195**, 279–288.

Fajardo RJ, Müller R (2001) Three-dimensional analysis of nonhuman primate trabecular architecture using micro-computed tomography. *Am J Phys Anthropol* **115**, 327–336.

Falster DS, Warton DI, Wright IJ (2003) *(S) MATR: Standardised Major Axis Tests and Routines*, Version 1.0. http://www.bio.mq.edu.ac/ecology/SMATR.

Fleagle JG (1999) *Primate Adaptation and Evolution*, 2nd edn. San Diego: Academic Press.

Frost HM (1990a) Skeletal structural adaptations to mechanical usage (SATMU): 1. Redefining Wolff's Law: the bone modeling problem. *Anat Rec* **226**, 403–413.

Frost HM (1990b) Skeletal structural adaptations to mechanical usage (SATMU): 1. Redefining Wolff's Law: the remodeling problem. *Anat Rec* **226**, 414–422.

Frost HM (2001) From Wolff's Law to the Utah Paradigm: insights about bone physiology and its clinical applications. *Anat Rec* **263**, 398–419.

Fyhrie DP, Carter DR (1986) A unifying principle relating stress to trabecular bone morphology. *J Orthop Res* **4**, 304–317.

Giunta RE, Biemer E, Müller-Gerbl M (2004) Ulnar variance and subchondral bone mineralization in the distal articular surface of the radius. *J Hand Surg* **29A**, 835–840.

Grynpas MD, Alpert B, Katz I, Lieberman I, Pritzker KPH (1991) Subchondral bone in osteoarthritis. *Calcif Tissue Int* **49**, 20–26.

Haapasalo H, Kannus P, Sievänen H, et al. (1998) Effect of long-term unilateral activity on bone mineral density of female junior tennis players. *J Bone Miner Res* **13**, 310–319.

Heinonen A, Oja P, Sievänen H, Pasanen M, Vuori I (1998) Effect of two training regimes on bone mineral density in healthy perimenopausal women: a randomized controlled trial. *J Bone Miner Res* **13**, 483–490.

Hoogbergen MM, Niessen WJ, Schuurman AH, Spauwen PHM, Kauer JMG (2002) Subchondral bone mineral density patterns representing the loading history of the wrist joint. *J Hand Surg* **27B**, 150–154.

Hunt KD, Cant JGH, Gebo DL, Rose MD, Walker SE (1996) Standardized descriptions of primate locomotor and postural modes. *Primates* **37**, 363–387.

Iwasaki N, Minami A, Miyazawa T, Kaneda K (2000) Force distribution through the wrist joint in patients with different stages of Kienböck's disease: using computed tomography osteoabsorptiometry. *J Hand Surg* **25A**, 870–876.

Kannus P, Haapasalo H, Sankelo M, Sievänen H, Oja P, Vuori I (1994) The site-specific effects of long-term unilateral activity on bone mineral density and content. *Bone* **15**, 279–284.

Kawcak CE, McIlwraith CW, Park RD (2001) The role of subchondral bone in joint disease. *Proc Am Assoc Equine Pratnr* **47**, 157–163.

Kikuchi Y, Udono T, Hamada Y (2003) Bone mineral density in chimpanzees, humans, and Japanese macaques. *Primates* **44**, 151–155.

Kontulainen S, Kannus P, Haapasalo H, et al. (1999) Changes in bone mineral content with decreased training in competitive young adult tennis players and controls: a prospective 4-year follow-up. *Med Sci Sports Exerc* **31**, 646–652.

Lanyon LE, Hampson WGJ, Goodship AE, Shah JS (1975) Bone deformation recorded in vivo from strain gauges attached to the human tibial shaft. *Acta Orthop Scand* **46**, 256–268.

Linsenmaier U, Kersting S, Schlichtenhorst K, et al. (2003) Functional CT imaging: Load-dependent visualization of the subchondral mineralization by means of CT osteoabsorptiometry (CT-OAM). *Röfo Fortschr Röntgenstr* **175**, 663–669.

de Margerie E (2002) Laminar bone as an adaptation to torsional loads in flapping flight. *J Anat* **201**, 521–526.

Martin RB, Burr DB, Sharkey NA (1998) *Skeletal Tissue Mechanics*. New York: Springer-Verlag.

Meirer R, Müller-Gerbl M, Huemer GM, et al. (2004) Quantitative assessment of periarticular osteopenia in patients with early rheumatoid arthritis: a preliminary report. *Scand J Rheumatol* **33**, 307–311.

Müller-Gerbl M, Putz R, Hodapp N, Schulte E, Wimmer B (1989) Computed tomography osteoabsorptiometry for assessing the density distribution of subchondral bone as a measure of long term mechanical adaptation in individual joints. *Skeletal Radiol* **18**, 507–512.

Müller-Gerbl M, Putz R, Hodapp N, Schulte E, Wimmer B (1990) Computed tomography osteoabsorptiometry: a method of assessing the mechanical condition of the major joints in a living subject. *Clin Biomech* **5**, 193–198.

Müller-Gerbl M, Putz R, Kenn R (1992) Demonstration of subchondral bone density patterns by three dimensional CT osteoabsorptiometry as a noninvasive method for in vivo assessment of individual long term stresses in joints. *J Bone Miner Res* **7** (Suppl. 2), 411–418.

Oizumi N, Suenaga N, Minami A, Iwasaki N, Miyazawa T (2003) Stress distribution patterns at the coracoacromial arch in rotator cuff tear measured by computed tomography osteoabsorptiometry. *J Orthop Res* **21**, 393–398.

Ortner DJ, Putschar WGJ (1981) Identification of pathological conditions in human skeletal remains. *Smithson Contrib Anthropol* **28**, 1–488.

Patel BA, Carlson KJ (2005) Hand postures, locomotion and bone density in the primate wrist. *Integrative Comp Biol* **44**, 545.

Pauwels F (1965) *Gesammelte Abhandlungen zur Biomechanik des Bewegungsapparates*. Berlin: Springer.

Pearson OM, Lieberman DE (2004) The aging of Wolff's 'Law': ontogeny and responses to mechanical loading in cortical bone. *Yrbk Phys Anthropol* **47**, 63–99.

Pidaparti RMV, Turner CH (1997) Cancellous bone architecture: advantages of nonorthogonal trabecular alignment under multidirectional joint loading. *J Biomech* **30**, 979–983.

Proctor KL, Adams WC, Shaffrath JD, Van Loan MD (2002) Upper-limb bone mineral density of female collegiate gymnasts versus controls. *Med Sci Sports Exerc* **34**, 1830–1835.

Radin EL, Paul IL, Tolkoff MJ (1970) Subchondral bone changes in patients with early degenerative joint disease. *Arthr Rheum* **13**, 400–405.

Radin EL, Paul IL, Rose RM (1972) Mechanical factors in osteoarthritis. *Lancet* **1**, 519–522.

Ruff CB, Leo FP (1986) Use of computed tomography in skeletal structure research. *Yrbk Phys Anthropol* **29**, 181–196.

Ryan TM, van Rietbergen B (2005) Mechanical significance of femoral head trabecular structure in *Loris* and *Galago* evaluated using micromechanical finite element models. *Am J Phys Anthropol* **126**, 82–96.

Schaffler MB, Burr DB (1984) Primate cortical bone microstructure: relationship to locomotion. *Am J Phys Anthropol* **65**, 191–197.

Skedros JG, Mason MW, Bloebaum RD (2001) Modeling and remodeling in a developing artiodactyls calcaneus: a model for evaluating Frost's Mechanostat hypothesis and its corollaries. *Anat Rec* **263**, 167–185.

Skedros JG, Hunt KJ, Hughes PE, Winet H (2003) Ontogenetic and regional morphologic variations in the turkey ulna diaphysis: implications for functional adaptation of cortical bone. *Anat Rec* **273A**, 609–629.

Smith RJ, Jungers WL (1997) Body mass in comparative primatology. *J Hum Evol* **32**, 523–559.

Swartz SM, Bertram JEA, Biewener AA (1989) Telemetered *in vivo* strain analysis of locomotor mechanics of brachiating gibbons. *Nature* **342**, 270–272.

Taaffe DR, Marcus R (1999) Regional and total body bone mineral density in elite collegiate male swimmers. *J Sports Med Phys Fitness* **39**, 154–159.

Tuttle RH (1972) Relative mass of cheiridial muscles in catarrhine primates. In *The Functional and Evolutionary Biology of Primates* (ed. Tuttle RH), pp. 262–291. Chicago: Aldine-Atherten.

Vose GP, Kubala AL (1959) Bone strength – its relationship to X-ray determined ash content. *Hum Biol* **31**, 261–270.

Wang Y, Wluka AE, Cicuttini FM (2005) The determinants of change in tibial plateau bone area in osteoarthritic knees: a cohort study. *Arthritis Res Ther* **7**, R687–R693.

Zollikofer CPE, Ponce de León MS (2005) *Virtual Reconstruction – a Primer in Computer-Assisted Paleontology and Biomedicine*. Hoboken, NJ: John Wiley & Sons, Inc.